Two-Dimensional Oscillatory Neural Network Based on Room-Temperature Charge-Density-Wave Devices

Alexander Khitun, *Member, IEEE*, Guanxiong Liu, *Member, IEEE*, and Alexander A. Balandin, *Fellow, IEEE*

***Abstract*—We propose an oscillatory neural network implemented with two-dimensional (2-D) tantalum disulfide devices operating in the change density wave regime at room temperature. An elementary cell of the network consists of two 1T-TaS_2 devices connected in series. Such a cell has a constant output and oscillatory states. All cells have the same bias voltage. There is a constant current flowing through the cell in the constant output mode. The oscillations occur at a certain bias voltage due to the electrical-field triggered metal-to-insulator transition owing to the changes in the charge-density-wave phase in the 1T-TaS_2 channel. Two 1T-TaS_2 devices oscillate out-of-phase when one of the devices is in the insulator phase while the other one is in the metallic state. The nearest-neighbor cells are coupled via graphene transistors. The cells are resistively coupled if the graphene transistor is in the ON state while they are capacitively coupled if the transistor is in the OFF state. The operation of the oscillatory neural network is simulated numerically for the 30 $\times$ 30 node network. We present the examples of pattern recognition on a template with the fixed coupling among the near-neighbor cells. We also present the results of our numerical modeling mimicking the Game of Life in the network with the time-varying coupling. The 2-D 1T-TaS_2 devices, utilized in the network, offer a unique combination of properties such as scalability, high operational frequency, fast synchronization speed, and radiation hardness, which makes them promising for both consumer electronic and defense applications.**

***Index Terms*—Charge density waves, oscillatory network, two-dimensional materials.**

I. Introduction

PRESENTLY, there is a strong motivation for development of a new generation of information processing systems, which function on the principles of biological or neuromorphic computing [1]. Such systems would drastically increase the computing efficiency in solving specific problems, particularly in image processing and pattern recognition. The neuromorphic computer, unlike the von Neumann computer, does not execute a list of commands, which constitute a program. Its major aim is not a general-purpose computation but rather special task data processing via the collective dynamics of the cells in the network [2]. The concept of a cellular neural network (CNN) was first formulated by Chua [3]. CNN is a two (three or more) dimensional array of mainly identical dynamical systems, called cells, which satisfy two properties: (i) most interactions are local within a finite radius, and (ii) all state variables are signals of continuous values. In subsequent works, the CNN paradigm evolved in many ways, and its computing capabilities in image processing and pattern recognition have been successfully demonstrated [4]–[7]. In recent years, the CNN concept attracted growing interest as a promising architecture for future information processing systems implemented with nanometer scale devices and structures [8]. Potentially, CNN comprising nano-cells will have a tremendous integration density, as well as specific architecture features originating from the unique output characteristics. A comprehensive review of nanoscale devices for the next generation computers is given in [9].

Oscillatory neural network is one of the promising approaches for development of the next generation computers. In such a network, an elementary cell comprises an oscillator circuit. The cells are locally coupled and may share a common node. The memorized and test patterns are encoded in the parameters of the oscillators. The collective behavior of the coupled oscillators is utilized for pattern recognition. There is a variety of nanoscale devices suitable for integration in an oscillatory network. An example of the oscillatory network with the coupled spin-torque oscillators is described in [10]. In general, an oscillatory network has two modes of operation: (i) the fixed point mode and (ii) the oscillatory mode. In the fixed point mode, the memories are stored as the fixed points of the network dynamics, whereas in the oscillatory mode they are encoded as the phase relations among individual oscillators.

A new impetus to the development of the oscillatory neural networks has recently appeared owing to emergence of the devices based on the metal-to-insulator transitions [11]–[14]. It opened a possibility of creating a new type of low-power, scalable, voltage-controlled oscillatory networks. In this work, we propose an oscillatory network based on two-dimensional (2D) tantalum disulfide (TaS_2) devices [15]. Specifically, we use 1T polytype of TaS_2, which undergoes the transition from a normal metallic phase to the charge density wave (CDW) phases at high

Manuscript received April 14, 2017; accepted May 26, 2017. Date of publication June 16, 2017; date of current version September 6, 2017. This work was supported in part by the National Science Foundation (NSF) Emerging Frontiers of Research Initiative (EFRI) 2-DARE Project Novel Switching Phenomena in Atomic MX2 Heterostructures for Multifunctional Applications (NSF EFRI 1433395). The review of this paper was arranged by associate editor P. E. Gaillardon. *(Corresponding author: Alexander Khitun.)*

The authors are with the Department of Electrical and Computer Engineering, Bourns College of Engineering, University of California, Riverside, Riverside, CA 92521 USA (e-mail: akhitun@ece.ucr.edu; guliu@ece.ucr.edu; balandin@ece.ucr.edu).

Color versions of one or more of the figures in this paper are available online at http://ieeexplore.ieee.org.

Digital Object Identifier 10.1109/TNANO.2017.2716845

temperature. The CDW state is a macroscopic quantum state formed via a periodic modulation of the electronic charge density accompanied by a periodic distortion of the atomic lattice in a quasi-1D or quasi-2D layered metallic crystal [16]–[19]. Some materials reveal several CDW phases with different transition temperatures. It is known that 1T-TaS_2 transforms from a normal metallic phase to an incommensurate CDW (IC-CDW) phase at 545 K, to a nearly commensurate CDW (NC-CDW) phase at 350 K and, finally, to a commensurate CDW (C-CDW) phase at 180 K [15]. Each phase transition is accompanied by a lattice reconstruction, which results in strong changes of the electrical properties of the material. The transition between the phases can be triggered by an applied voltage. We used 1T-TaS_2 as the device channel material where electrical current is switched by inducing transition between IC-CDW and NC-CDW states [15]. The integration of two 1T-TaS_2 devices provides a simple, miniaturized, voltage-controlled oscillator. A large number of 1T-TaS_2 oscillators can be integrated in a network, where the coupling between the oscillators can be controlled by the graphene transistors.

The rest of the paper is organized as follows. In the next Section II, we outline the structure and fabrication of 1T-TaS_2 - graphene devices, and present experimental current-voltage (I-V) characteristics. In Section III, we describe the oscillatory neural network and present results of the numerical simulations illustrating the operation and collective behavior in the network. The experimental I-Vs are used as input data for our numerical model. The discussion and conclusions are given in Sections IV and V, respectively.

II. Device Structure and Characteristics of 1T-TaS_2 – Based Oscillator

Metal-insulator-transition (MIT) is the physical mechanism leading to the self-sustained oscillations. The simplest oscillatory circuit consist of one MIT device and a passive resistor as described in [11]. In order to demonstrate the self-sustained oscillations in 1T-TaS_2 – based circuit, we build a prototype consisting of the 1T-TaS_2 channel connected in series with an off chip resistor, D-R configuration. The 1T-TaS_2 channel experiences switching between electrically conducting (IC-CDW) and resistive (NC-CDW) states as the voltage across the threshold value $\mathrm{V_{TH}}$. The 1T-TaS_2 channel is capped with hexagonal boron nitride (h-BN) layer, which serves as a protective capping. A schematic of the oscillator device structure and an optical microscopy image of a typical fabricated device are shown in Fig. 1(A) and (B), respectively.

We fabricated a number of prototype devices for the proof-of-concept demonstration using mechanical exfoliation and transfer process. Briefly, the fabrication can be summarized in the following steps. A thin 1T-TaS_2 layer is exfoliated on SiO_2/Si substrate while an h-BN thin layer is exfoliated from the bulk material onto the PDMS stamp. The stamp is then used to align and transfer h-BN on top of 1T-TaS_2 film [4]–[6]. In the proposed devices the metal contacts to 1T-TaS_2 are made in the edge contact configuration. The oscillations are observed when applying DC bias to the D-R circuit. As the voltage across 1T-TaS_2 channel exceeds $\mathrm{V_{TH}}$, the oscillation occurs at the output port. The current-voltage characteristics of 1T-TaS_2 device and the oscillation waveform of the D-R circuit are shown in Fig. 2. The load resistance is 1 kΩ, DC bias is 4.21 V, and the frequency is 2 MHz.

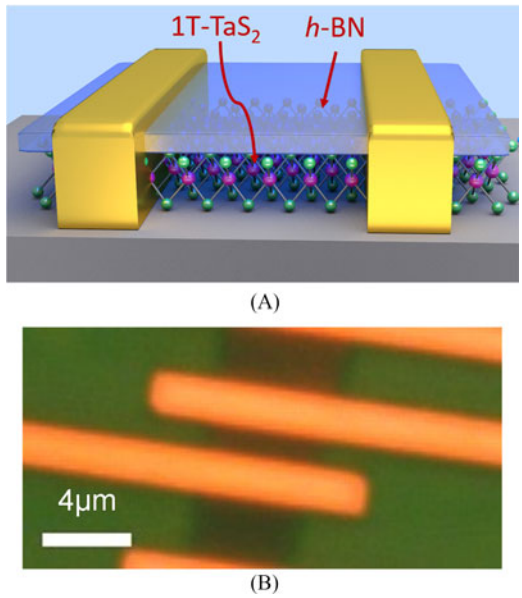

Fig. 1. (A) Structure of 1T-TaS_2 device. 1T-TaS_2 thin film is fully covered with *h*-BN, which acts as a protective layer against oxidation. (B) The optical image of a typical 1T-TaS_2 device.

III. Device Model and Results of Simulations

We adopt the metal-insulator-transition (MIT) device model from [11]. The model has been validated with our experimental data. In the framework of this model, the device has two resistance states R_H and R_L, where R_H is the high resistance corresponding to the insulator state, and R_L is the low resistance corresponding to the metallic state. The switching among the states is triggered by the voltage across the device. There are two threshold voltages v_h and v_l corresponding to the transitions between the metal and insulator phases. The resistance changes to a metallic (R_L) state as the voltage exceeds the higher threshold v_h. The change to the insulating (R_H) state occurs when the voltage exceeds the lower threshold v_l. The thresholds v_h and v_l are not equal, i.e. there is hysteresis in the switching with $\mathrm{v}_l < \mathrm{v}_h$. Such a simple model describes well the I-V characteristics of VO_2 MIT devices [11].

The simplest way of building an oscillator circuit is to combine MIT device (D) with a resistor (R) in series as shown in Fig. 3(A). The phase space of a single D-R oscillator is shown in Fig. 3(B). As in [11], we define conductance $\mathrm{g_{di}} = 1/R_H$, $\mathrm{g_{dm}} = 1/R_L$, $\mathrm{g}_S = 1/R_S$, where subscript *d* denotes the state dependent device conductance and *m/i* denotes the metallic/insulating state respectively, R_s correspond to the linear resistor. Effective charging happens through $\mathrm{g_{dm}}$ and whereas effective discharging happens only through $\mathrm{g_s}$. The equation for the single D-R oscillator dynamics can be described by the following set of piecewise linear differential equations written

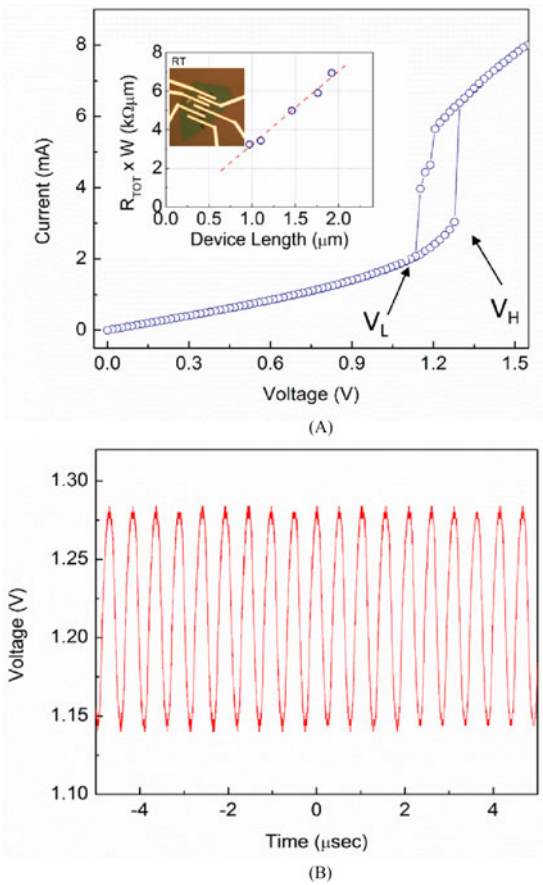

Fig. 2. (A) Current-voltage characteristics of 1T-TaS_2 device at room temperature. The CDW phase transition can be triggered by applying voltage beyond the threshold level. The inset shows the photo of the device and experimental data on the device resistance. (B) the oscillation waveform of a D-R circuit. Load resistance is 1 kΩ, DC bias is 4.21 V.

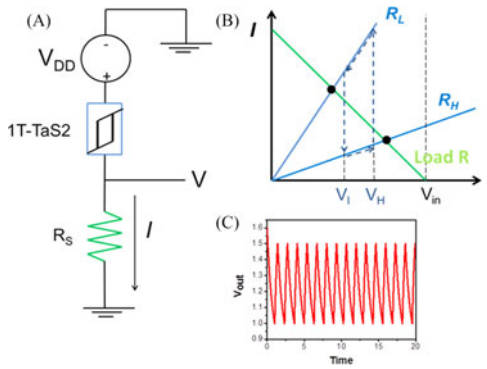

Fig. 3. (A) Schematics of an oscillator circuit realized with a MIT device in series with a resistor (D-R configuration). (B) Phase space of the device in a single (D-R) oscillator. (C) Results of numerical modeling showing the output of the (D-R) oscillator.

as [11]:

$$cv' = \begin{cases} (v_{\rm dd} - v)g_{\rm dm} - vg_S \\ -vg_S \end{cases} \quad (1)$$

The D-R circuit produces an oscillating output at a certain combination of the resistances R_H, R_L, R_S and the bias voltage $v_{\rm dd}$, as explained in Fig. 1(B). The lines with the slopes R_H and R_L are the regions of operation of the device in the insulating and metallic states, respectively. The intersection of these lines with the load line, due to the series resistance R_S, gives the stable points of the system in the two states. In order to obtain the self-sustained oscillations, the stable points in each state should lie outside the region of operation, i.e. outside the region defined by vertical lines passing through the transition points. In this case, MIT device has a phase transition before the circuit reaches the stable point. Fig. 3(C) shows the results of the numerical modeling illustrating the oscillating output of the D-R oscillator. Hereafter, we depict all values in the normalized units R_0, I_0, and V_0, where $I_0 = V_0/R_0$. In our numerical simulations, we used the following set of parameters: $\mathrm{v}_l = 1\,V_0$, $\mathrm{v}_h = 2\,V_0$, $R_H = 2.73\,R_0$, $R_L = 0.67\,R_0$, $R_S = 1\,R_0$. We intentionally enlarged the ratio of the high and low threshold voltages $v_l/v_h = 2$ compared to the experimental data $\mathrm{v}_l/\mathrm{v}_h \sim 1.3$ as shown in Fig. 2. The ratio of the $R_H/R_L = 4$ is also increased $\times 2$ compared to the experimental data $\mathrm{R}_H/\mathrm{R}_L \sim 2$ in order to speed up the numerical simulations.

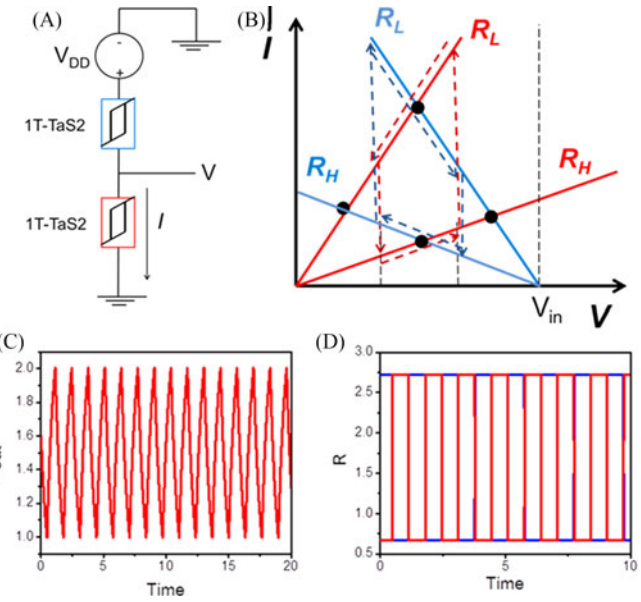

Fig. 4. (A) Schematics of relaxation oscillator circuit realized with two MIT devices connected in series - (D-D) configuration. (B) Phase space of the D-D oscillator. (C) Results of numerical modeling showing the output of the (D-D) oscillator. (D) Resistance states of the 1T-TaS_2 devices as a function of time. The devices are mostly in the different resistance states (i.e. if one of the devices is in the high-resistance state, the second one is in the low resistance state).

Following the same methodology, one can write the equation for D-D oscillator circuit as shown in Fig. 4(A):

$$cv' = \begin{cases} (v_{\rm dd} - v)g_{\rm 1dm} & \text{charging} \\ -vg_{2dM} & \text{discharging} \end{cases} \quad (2)$$

The only difference from the D-R case is that the effective charging happens through $\mathrm{g}_{\rm 1dm}$ and the effective discharging through $\mathrm{g}_{\rm 2dm}$. The conditions leading to the self-sustained oscillation are illustrated in Fig. 3(B). Due to the symmetry in

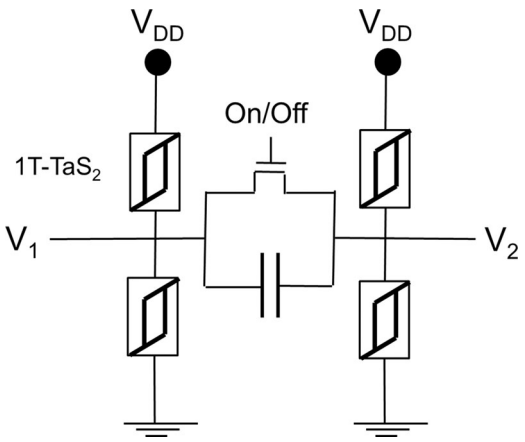

Fig. 5. Schematics of two D-D coupled oscillators. The type of coupling is controlled by the transistor. In the On state, the resistive coupling dominates forcing the two oscillators to oscillate in phase. In the Off state, the capacitive coupling comes to the stage by introducing a π-phase shift between the oscillators.

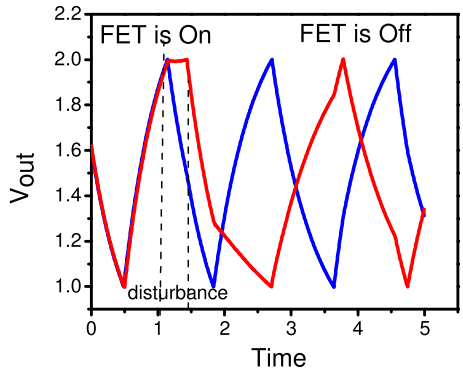

Fig. 6. Results of the numerical modeling for two D-D coupled oscillators shown schematically in Fig. 5. The blue and the red curves show V_1 and V_2, respectively. The simulation starts with the transistor On (resistive coupling). Then, transistor is turned Off and a small perturbation $(0.1\mathrm{V}_0)$ is applied to the one of the oscillators at $\mathrm{Time} = 1\mathrm{t}_0$. The system switches to the out-of-phase oscillation.

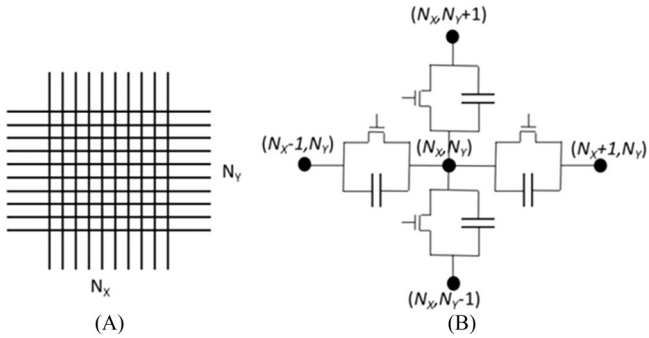

Fig. 7. (A) Schematics of 2D network consisting of D-D coupled oscillators. (B) Elementary cell of the network comprising nearest-neighbor coupled oscillators. The coupling between the oscillators is controlled by the junction transistors.

I-V characteristics, two MIT devices are biased in such a way, that the phase transition in each device occurs before the system reaches one of the four stable points. In this scenario, as one of the MIT devices changes its state from metallic to insulator, the second MIT device has phase transfer from insulator to metal state, and vice versa. As a result, the system of two MIT devices forms a *complementary pair*, where one of the devices is in high resistance state, while the other is in low resistance state. Fig. 4(C) shows the results of numerical modeling illustrating the switch between the resistance states for MIT devices in D-D configuration. Compare to the R-D configuration, D-D circuit possesses a lower leakage current, similar to the well-established complementary metal oxide semiconductor (CMOS).

There are different possible ways for oscillator coupling. There are two extreme cases of the purely resistive and purely capacitive coupling. In the case of the purely resistive coupling, two oscillators are tending to oscillate in phase. In contrast, the purely capacitive coupling makes the two oscillators to oscillate out of phase. The dynamics of purely resistive and purely capacitive coupled D-D oscillators are described in details in [11]. In this work, we propose a combination of the MIT-based oscillators and a graphene transistor as shown in Fig. 5. Two D-D circuits are coupled via the resistance R_C and the capacitance C_C. The mutual capacitance C_c is fixed after the fabrication, while the coupling resistance R_C is controlled by the state of the graphene transistor (G-FET). In the On state, the resistive coupling dominates, forcing the two oscillators to oscillate in phase. In the Off state, the capacitive coupling comes to the stage by introducing a π-phase shift between the oscillators. It is important to note, that two capacitively coupled D-D oscillators may occur in a meta-stable state (i.e. in-phase oscillation) till an external perturbation will make the system to evolve towards the stable out-of-phase state. This transition is illustrated by the numerical modeling in Fig. 6. We consider two D-D coupled oscillators as shown in Fig. 5. The red and the blue curves in Fig. 6 correspond to V_1 and V_2, respectively. The simulations are started with the transistor in state On. The later corresponds to the in-phase oscillation of V_1 and V_2. Switching the transistor to the state Off makes the capacitive coupling dominant. The later corresponds to the out-of-phase oscillations of V_1 and V_2. As it can be seen from Fig. 6, it takes only a couple of cycles for the in-phase to the out-of-phase transition. A more detailed analysis of the relaxation dynamics including numerical modeling can be found in [11]. The introduction of a transistor controlling the coupling between the MIT-based oscillators in a network opens a number of intrigue possibilities for engineering special templates for data processing. In the rest of this work, we show some examples of the proposed approach.

As a testbed, we consider a 30×30 template of the identical D-D coupled oscillators (i.e. as shown in Fig. 4). An elementary cell of the network is shown in Fig. 7, where a D-D oscillator is connected to the four nearest-neighbor D-D oscillators. The position of the cell in the network is defined by the two numbers N_X and N_Y. The state of the cell is assigned to the voltage $V(N_X, N_Y)$ as depicted in Fig. 7(B). There are four junction transistors connecting the central oscillators with the four neighbors. As in Fig. 5, the states of these transistors define the type of coupling (e.g. the On state of the transistor corresponds to the inter-cell resistance of 0.1 R_0, the Off state corresponds to the inter-cell resistance 10 R_0). For instance, oscillator (N_X, N_Y) can be capacitively coupled to the oscillator (N_{X+1}, N_Y) but resistively coupled to the other neighbors.

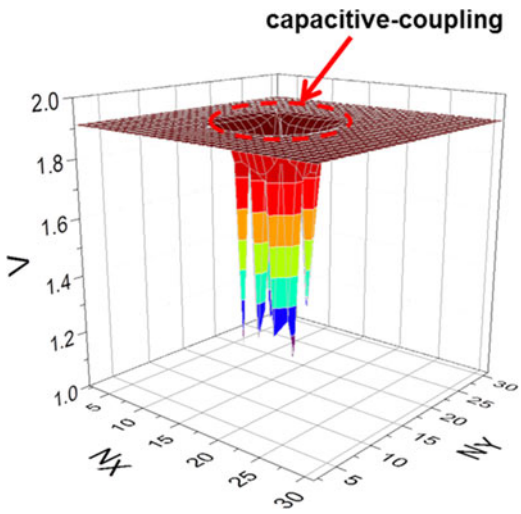

Fig. 8. Results of numerical simulations. The color surface shows the voltage map in the 2-D array of oscillators. Nx and N_Y depict the position of the oscillator in the network. The oscillators in the center of the network around $N_X = 15$, $N_Y = 15$ with radius 7, are capacitively coupled. The rest of the oscillators are resistively coupled.

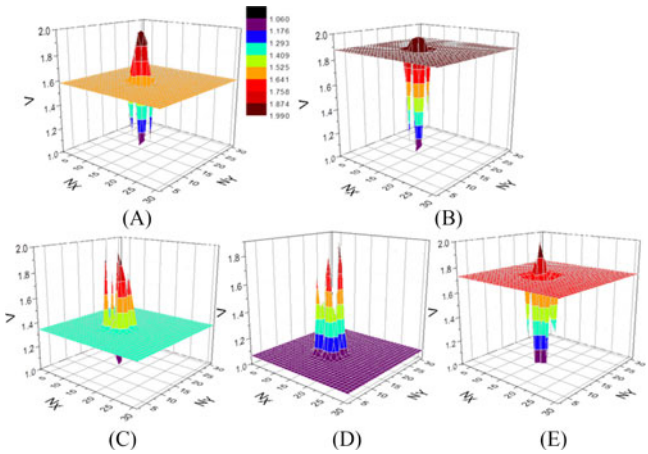

Fig. 9. Results of numerical simulations showing the dynamics in the template with capacitively- (center) and resistively- (out of the central region) coupled oscillators. The graphs (A–E) are the snapshots of the network voltage map taken with the time step 0.05 [RC].

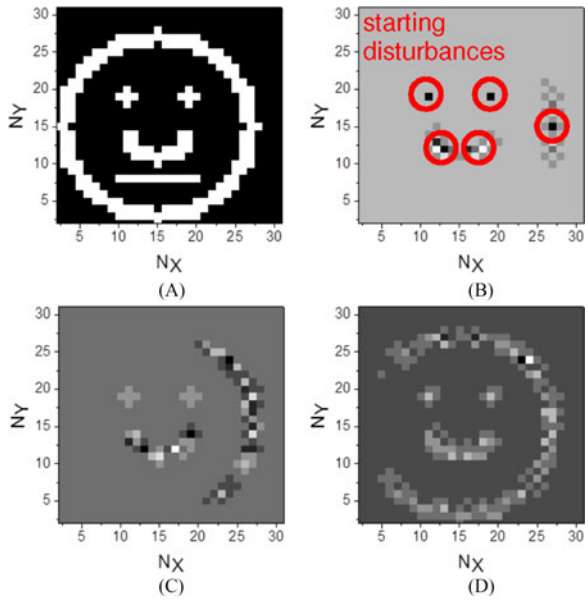

Fig. 10. (A) Connectivity map. White and black markers correspond to capacitively and resistively connected cells. (B) Results of numerical modeling. The simulations start with all cells oscillating in-phase. A small perturbation $(0.1\,V_0)$ is applied to the selected cells shown within the red circles. (C) Voltage map in oscillatory 100 cycles. (D) Voltage map in oscillatory 150 cycles.

As the first example, let us consider a template with two regions consisting of the capacitively and resistively coupled oscillators. The capacitively coupled oscillators are located in the center of the template (i.e. all oscillators around (15,15) with radius 7). All the oscillators outside this region are resistively coupled. The states of the transistors are fixed and are not changing during simulations. We assume all the oscillators to be biased with the same voltage $V_{DD} = 3V_0$. Such a network demonstrates an interesting dynamics, which is illustrated by numerical modeling.

The color surface in Fig. 8 presents the results of numerical modeling. The color surface shows the voltage map in the 2-D array of oscillators. The N_X and N_Y values depict the position of the oscillator in the network. The color depicts the voltage of the cell. The resistively coupled oscillator oscillate in phase (i.e. the same voltage in every moment of time), while the capacitively-coupled oscillators in the center oscillate out-of-phase. In this case, the bulk of the resistively coupled oscillators constitute a background with a vortex-like center. In Fig. 9, we show the sequence of voltage maps calculated with the time interval of $0.05t_0$, where $t_0 = R_0C_0$, where $C_0 = 0.01$. Let us consider the dynamic of the resistively-coupled background (i.e., the cells outside the central region). For example, one can trace V(2, 2) through Fig. 9(A)–(D): $1.6\,V_0$, $1.9\,V_0$, $1.3\,V_0$, $1.1\,V_0$, and $1.7\,V_0$. Next, one can trace the cell voltage for the cells inside the central region. There are the same amplitude margins for the voltage oscillations (i.e., from $1.1\,V_0$ to $1.9\,V_0$). However, the capacitively-coupled nearest-neighbor cells oscillate out-of-phase. This dynamics resembles a magnetic vortex, where the position of magnetization is copied by the phase of oscillation. In contrast to the steady-state magnetic vortexes, this artificial vortex in the sea of coupled oscillators does not show any stead-state phase distribution. The phase difference between any oscillator in the center and any oscillator out of the central region varies with time. This phase evolution is defined by the set of electric characteristics as well as the geometry of the capacitively-coupled region.

Pattern recognition is one of the practically important operation which can be realized with CNN [20]. In this part, we present the results of numerical modeling illustrating the possibility of pattern recognition in the network based on MIT devices. The main idea is to exploit the transition from the metastable to the stable oscillatory states in a network of capacitively-coupled oscillators. Let us consider a network with specially designed coupling (i.e., controlled by the transistors). The connection map is shown in Fig. 10(A). The black and the white color cells correspond to the resistively and capacitively-coupled cells, respectively. All of the cells are biased by the same volt-

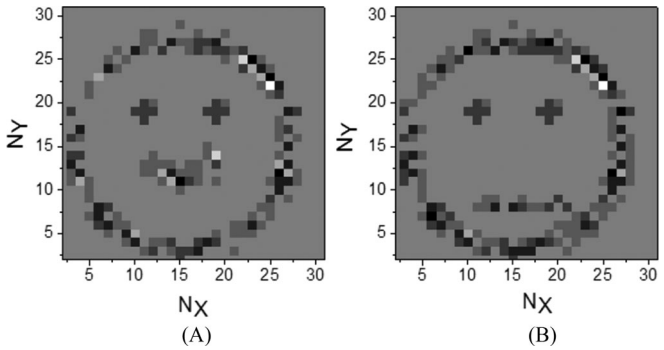

Fig. 11. Results of numerical simulation showing the final voltage map after oscillatory 200 cycles. The simulations are carried out for the *same connectivity map* as shown in Fig. 7 (A) Smiling face appears with the initial disturbances applied to the cells (11, 19), (19, 19), (27, 15), (15, 12). (B) Sad face appears with the initial disturbances applied to the cells (11, 19), (19,19), (27, 15), (15, 8).

age $V_{DD} = 3V_0$. In the beginning, all the cells oscillate in-phase (i.e., all the capacitively–coupled cells are in the metastable state). Next, we introduce a small ($0.1\ V_0$) disturbance to the selected cells. The disturbance triggers the relaxation of the capacitively-coupled cells to the out-of-phase state. The switching from the in-phase to the out-of-phase states occurs in a cellular-automata fashion through the chains of capacitively-coupled cells. In Fig. 10(B)–(D), we present the results of numerical simulations showing signal propagation through the network. The gray-scale color maps show the distribution of the cell voltages in the network. Fig. 10(B), it is shown the voltage map as the $0.1V_0$ disturbance is applied to the cells with the following (N_X, N_Y) coordinates: (11, 19), (19, 19), (27, 15),(15, 12). The disturbance triggers the cell relaxation. Fig. 10(B)–(D) show the evolution of the voltage map in time. Finally, the map stabilizes with the distribution resembling a smiling face as shown in Fig. 11(A). It should be noted, that the final network state is defined by the initial connectivity map [e.g. as shown in Fig. 10(A)] as well as the set of the selected cells where the disturbance is applied. For instance, changing the set of the input cells to (11, 19), (19, 19), (27, 15), (15, 8) leads to the different final state as shown in Fig. 11(B).

The results of numerical modeling presented in Figs. (8)–(11) are obtained for the fixed interconnection templates, where the type of coupling (e.g., resistive or capacitive) between the nearest-neighbor cell does not change in time. More sophisticated and interesting is the case where the type of coupling between the cells is a function of the cell voltage. For example, the type of coupling between the cells with coordinates (7, 7) and (7, 8) depends on the voltage of the cell (24, 24). The latter is practically feasible by connecting the cells output (e.g., V_1 or V_2 in Fig. 5) to the gates of the transistors. The change in the connectivity map leads to the variety of the evolving in time phase patterns. Finally, we present the results of numerical modeling showing the Game of Life in the network of coupled 1T-TaS_2 oscillators The Game of Life is a special version of cellular automation invented by the J.H. Conway in 1970 [21]. It consists of a collection of cells which may have two or more states (e.g. black and white). The cells change their states ac-

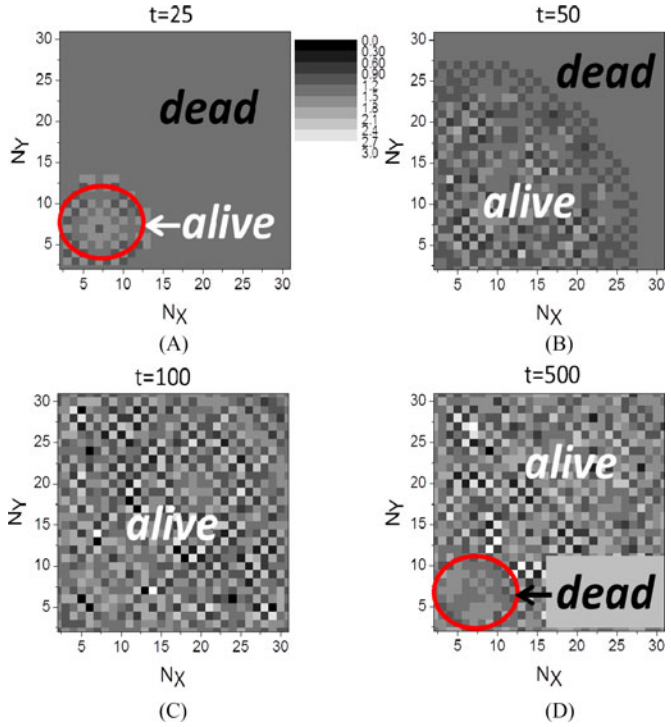

Fig. 12. Results of numerical simulations showing system evolution. (A) Starting configurations. There is a group of capacitively-coupled oscillators in the left bottom corner – cell alive. All other oscillators oscillate in-phase – dead cells. (B) System evolves by driving more capacitively-coupled oscillators out of the metastable state. (C) Culmination of living cell growth. As the living cells reach the top right corner, it triggers the coupling switch for the oscillators in the left bottom corner. The oscillators become resistively coupled. (D) The oscillators in the left bottom corner oscillate in-phase, which symbolizes cell death.

cording to the set of rules, which results in a system evolution mimicking living cell birth, multiplication and death. Depending on the initial conditions, the cells may form various patterns throughout the evolution. The Game of Life offers an original way of implementing complex Boolean operators in the space-time dynamics and presents a testbed for artificial intelligence development. In our case, we define living cell as a local group of oscillators in the out-of-phase state. The dead cell is a group of oscillators in the in-phase state. The main idea of our approach is to construct a system of oscillators where the type of coupling in one place of the network depends on the oscillatory states in the other parts of the network.

In order to illustrate this idea, we present the results of numerical modeling on the 30×30 oscilaltor network. In Fig. 12(A), it is shown a starting oscillator configuration. There is a circular region consisting of capacitively -coupled oscillators in the left bottom corner (i.e., around (7, 7)). The nearest-neighbor oscillators in this region oscillate out-of-phase, so we recognize this ensemble of oscillators as a cell alive. The rest of the network including capacitively as well as resistively-coupled cells oscilalte in-phase. The system starts to evolve as the group of capacitively-coupled oscillators around cell (7, 7) triggers the relaxation from the in-phase to out-of-phase oscilaltion. This process of evolution or spreading of alive cells is illustrated in Fig. 12(B). This part is similar to the case as shown in

Fig. 10(B)–(D). The process continues till all of the capacitively-coupled oscillators are out of the metastable state. Fig. 10(C) shows the ultimate system state filled with all cells alive. The system is programmed such a way that the oscillator at position (24, 24) controls the coupling between the oscillators in the group around (7, 7). As soon as the output voltage of cell (24, 24) exceeds certain threshold value (e.g., $V = 2V_0$), it makes all the switches in the region in the position On (i.e., resistive coupling). As a result of this transformation, the oscillators in the bottom left corner start to oscillate in-phase, and the initial cell alive change its state to dead. This final stage is shown in Fig. 10(D). Thus, the evolution of the network exibits three major processes – the attributes of the Game of Life: birth, growth and death. The presented results are aimed to show the possibilities of CNN based on coupled 1T-TaS_2 oscillators which allows us to utilize both local and distant cell coupling.

IV. Discussion

There are several advantages inherent to 1T-TaS_2 – graphene devices, including scalability, high operation frequency, fast synchronization, voltage control of the operation frequency, flexibility, and radiation hardness. However, G-FETs show relatively low $I_{\rm on}/I_{\rm off}$ ratio due to the absence of the energy band gap, which significantly narrows perspectives of using G-FETs in conventional digital logic [22]. In our proposed architecture, G-FETs are utilized for the oscillatory circuits coupling, where the $I_{\rm on}/I_{\rm off}$ ratio of 100 is sufficient for switching between the resistive and capacitive regimes. The type of coupling between the D-D oscillators, shown in Fig. 5, depends on the ratio between the G-FET resistance $R_{G-\rm FET}$ and the capacitor reactance $X_C = 1/2\pi fC$ $\alpha = R_{G-\rm FET}/X_C$. The restive coupling is dominant if $\alpha\langle\langle 1$, and the capacitive coupling is dominant if $\alpha\rangle\rangle 1$. The operation frequency f and the coupling capacitance C can be adjusted to provide resistive coupling for G-FET On state, and capacitive coupling for G-FET Off state. For example, taking R(On) = 1 kΩ, R(Off) = 100 kΩ, $f = 1$ GHz, C = 15 fF, $\alpha\langle\langle 1$ for the On state, and $\alpha\rangle\rangle 1$ for the Off state.

It is known that G-FETs can operate at the very high frequencies of hundreds of GHz [23], [24]. The switching 1T-TaS_2 channel oscillators, based on transitions between IC-CDW and NC-CDW phases, can potentially reach frequencies of up to ∼1 THz [25]. These considerations suggest that the frequency of operation of 1T-TaS_2 – G-FET devices can be increased substantially compared to the one demonstrated experimentally. In the present experiments, the frequency is limited by the extrinsic RC time constants of the probe station measurement apparatus. The intrinsic resistances and capacitances can be reduced by scaling. It is important to note that 1T-TaS_2 – based oscillator circuits do not require any micro- or nano-inductor components, which is one of the major issue for integrated magnetics [26]. An additional advantage of the selected material systems is that graphene and h-BN layers in the device structure have extremely high thermal conductivity [27], [28], and, as a result, act as heat spreaders. Graphene is a very promising candidate for applications in flexible electronics due to its high carrier mobility and mechanical flexibility [29]. The combination of graphene transistors with 2D 1T-TaS_2 may pave a road towards the new generation of flexible circuits. For some applications, e.g. deep-space probes, radiation hardness is an important metric. The considered 1T-TaS_2 – G-FETs are all-metallic devices, which are less susceptible to radiation damage than semiconductors. There have been a number of attempts to implement all-metallic switches and circuits, ranging from metal dot single electron transistors, to metallic carbon nanotube devices, and metallic nanowire transistors [30]–[34]. Our CDW devices belong to the same class of devices that do not use semiconductor components. The results of our numerical modeling show fast synchronization among the coupled oscillators. It takes only a couple of cycles for the 1T-TaS_2 – graphene device for transition from the in-phase to the out-of-phase oscillatory states. This is another important benefit of the proposed technology. The presented data suggests that overall, the unique output characteristics of 1T-TaS_2 devices are of great potential for implementation in phase-based logic devices using oscillatory nano-systems [35].

V. Conclusion

We presented a design of an oscillatory neural network based on integrated 1T-TaS_2 – graphene devices. The oscillations are driven by 1T-TaS_2 channel switching between two CDW states. Graphene FETs are used for coupling between the 1T-TaS_2-based oscillatory cells. We illustrated the dynamics of the proposed network by numerical modeling of a network comprising 32 × 32 cells, where each cell consists of two 1T-TaS_2 devices. The type of coupling (e.g. capacitive or resistive) between the nearest-neighbor cells is controlled by the G-FETs. We demonstrated examples of pattern recognition using 1T-TaS_2-based network by numerical modeling. The results are obtained for a template with the fixed coupling among the near-neighbor cells. We also present the results of numerical modeling mimicking the Game of Life in the network with the time-varying coupling. The results of the numerical simulations reveal potential of the proposed network for general and special task data processing. The integrated 1T-TaS_2 – graphene devices possess a unique combination of properties such as scalability, high operational frequency, fast synchronization speed, radiation hardness, which makes them well suited for application in oscillatory networks.

Acknowledgment

The 1T-$TaSe_2$ crystals used for fabrication of the prototype devices were provided by Prof. Tina T. Salguero, University of Georgia.

References

[1] V. P. Shmerko and S. N. Yanushkevich, "Natural computing paradigms for predictable nanoelectronics," *J. Comput. Theor. Nanosci.*, vol. 7, pp. 303–324, Feb. 2010.

[2] F. C. Hoppensteadt and E. M. Izhikevich, "Oscillatory neurocomputers with dynamic connectivity," *Phys. Rev. Lett.*, vol. 82, pp. 2983–2986, Apr. 1999.

[3] L. O. Chua and L. Yang, "Cellular neural networks: theory," *IEEE Trans. Circuits Syst.*, vol. 35, no. 10, pp. 1257–72, Oct. 1988.

[4] T. Matsumoto, L. O. Chua, and T. Yokohama, "Image thinning with a cellular neural network," *IEEE Trans. Circuits Syst.*, vol. 37, no. 5, pp. 638–40, May 1990.

[5] K. R. Krieg, L. O. Chua, and L. Yang, "Analog signal processing using cellular neural networks," in *Proc. 1990 IEEE Int. Symp. Circuits Syst.*, New York, NY, USA, 1990, vol. 2, pp. 958–61.
[6] T. Roska, T. Boros, P. Thiran, and L. O. Chua, "Detecting simple motion using cellular neural networks," in *Proc. 1990 IEEE Int. Workshop Cellular Neural Netw. Appl*, New York, NY, USA, 1990, pp. 127–38.
[7] P. L. Venetianer, F. Werblin, T. Roska, and L. O. Chua, "Analogic CNN algorithms for some image compression and restoration tasks," *IEEE Trans. Circuits Syst. I, Fundam. Theory Appl.*, vol. 42, no. 5, pp. 278–84, May 1995.
[8] "International technology roadmap for semiconductors, emerging research devices," 2013. [Online]. Available: http://www.itrs.net/Links/2013ITRS/2013Chapters/2013ERD.pdf
[9] D. E. Nikonov and I. A. Young, "Overview of beyond-CMOS devices and a uniform methodology for their benchmarking," *Proc. IEEE*, vol. 101, no. 12, pp. 2498–2533, Dec. 2013.
[10] G. Csaba *et al.*, "Spin torque oscillator models for applications in associate memories," in *Proc. 2012 13th Int. Workshop Cellular Nanoscale Netw. Appl.*, 2012, pp. 1–2.
[11] A. Parihar, N. Shukla, S. Datta, and A. Raychowdhury, "Synchronization of pairwise-coupled, identical, relaxation oscillators based on metal-insulator phase transition devices: A model study," *J. Appl. Phys.*, vol. 117, Feb. 7, 2015, Art. no. 054902.
[12] N. Shukla *et al.*, "Synchronized charge oscillations in correlated electron systems," *Sci. Rep.*, vol. 4, May 2014, Art. no. 4964.
[13] N. Shukla, S. Datta, A. Parihar, and A. Raychowdhury, Eds., *Future Trends in Microelectronics: Journey into the Unknown*. New York, NY, USA: Wiley, 2016.
[14] T. C. Jackson, A. A. Sharma, J. A. Bain, J. A. Weldon, and L. Pileggi, "Oscillatory neural networks based on TMO nano-oscillators and multilevel RRAM cells," *IEEE J. Emerging Select. Topics Circuits Syst.*, vol. 5, no. 2, pp. 230–241, Jun. 2015.
[15] G. Liu, B. Debnath, T. R. Pope, T. T. Salguero, R. K. Lake, and A. A. Balandin, "A charge-density-wave oscillator based on an integrated tantalum disulfide–boron nitride–graphene device operating at room temperature," *Nature Nanotechnol.*, vol. 11, pp. 845–850, 2016.
[16] G. Gruner, "The dynamics of charge-density waves," *Rev. Modern Phys.*, vol. 60, pp. 1129–1182, Oct. 1988.
[17] T. L. Adelman, S. V. Zaitsevzotov, and R. E. Thorne, "Field-effect modulation of charge-density-wave transport in NBSE3 and TAS3," *Phys. Rev. Lett.*, vol. 74, pp. 5264–5267, Jun. 1995.
[18] S. V. Zaitsev-Zotov, "Finite-size effects in quasi-one-dimensional conductors with a charge-density wave," *Phys.-Uspekhi*, vol. 47, pp. 533–554, Jun. 2004.
[19] D. E. Moncton, J. D. Axe, and F. J. Disalvo, "Study of superlattice formation in 2H-NBSE2 and 2H-TASE2 by neutron-scattering," *Phys. Rev. Lett.*, vol. 34, pp. 734–737, 1975.
[20] L. O. Chua and T. Roska, Eds., *Cellular Neural Networks and Visual Computing: Foundations and Applications*. New York, Ny, USA: Cambridge Univ. Press, 2002.
[21] M. Gardner, "Mathematical games: The fantastic combinations of John Conway's new solitaire game life," *Sci. Amer.*, vol. 223, pp. 120–123, 1970.
[22] P. Avouris, "Graphene: Electronic and photonic properties and devices," *Nano Lett.*, vol. 10, pp. 4285–4294, Nov. 2010.
[23] Y. M. Lin *et al.*, "Wafer-scale graphene integrated circuit," *Science*, vol. 332, pp. 1294–1297, Jun. 2011.
[24] Y. Q. Wu *et al.*, "High-frequency, scaled graphene transistors on diamond-like carbon," *Nature*, vol. 472, pp. 74–78, Apr. 2011.
[25] L. Perfetti *et al.*, "Femtosecond dynamics of electronic states in the Mott insulator 1T-TaS(2) by time resolved photoelectron spectroscopy," *New J. Phys.*, vol. 10, May 2008, 053019 (17pp).
[26] C. O. Mathuna, N. N. Wang, S. Kulkarni, and S. Roy, "Review of integrated magnetics for power supply on chip (PwrSoC)," *IEEE Trans. Power Electron.*, vol. 27, no. 11, pp. 4799–4816, Nov. 2012.
[27] A. A. Balandin, "Thermal properties of graphene and nanostructured carbon materials," *Nature Mater.*, vol. 10, pp. 569–581, Aug. 2011.
[28] I. Jo *et al.*, "Thermal conductivity and phonon transport in suspended few-layer hexagonal boron nitride," *Nano Lett.*, vol. 13, pp. 550–554, Feb. 2013.
[29] W. J. Zhu *et al.*, "Graphene radio frequency devices on flexible substrate," *Appl. Phys. Lett.*, vol. 102, Jun. 2013, Art. no. 233102.
[30] A. N. Korotkov, R. H. Chen, and K. K. Likharev, "Possible performance of capacitevely coupled single-electron transistors in digital circuits," *J. Appl. Phys.*, vol. 78, pp. 2520–2530, Aug. 1995.
[31] V. A. Zhukov and V. G. Maslov, "A model of a metallic quantum nanotransistor with a Coulomb-blockage gate in "magic" Au55 and Ag55 nanocrystals with speed of 1011 Hz," *Russ. Microelectron.*, vol. 42, pp. 102–112, 2013.
[32] V. A. Krupenin, A. B. Zorin, M. N. Savvateev, D. E. Presnov, and J. Niemeyer, "Single-electron transistor with metallic microstrips instead of tunnel junctions," *J. Appl. Phys.*, vol. 90, pp. 2411–2415, Sep. 2001.
[33] Q. H. Liu *et al.*, "All-metallic high-performance field effect transistor based on telescoping carbon nanotubes: An ab initio study," *J. Phys. Chem. C*, vol. 115, pp. 6933–6938, Apr 2011.
[34] H. H. Cheng, C. N. Andrew, and M. M. Alkaisi, "The fabrication and characterisation of metallic nanotransistors," *Microelectronic Eng.*, vol. 83, pp. 1749–1752, Apr.–Sep. 2006.
[35] W. Tianshi and J. Roychowdhury, "PHLOGON: PHase-based LOGic using oscillatory nano-systems," Dept. Elect. Eng. Comput. Sci., Univ. California, Berkeley, CA, USA, 2014.

Alexander Khitun received the B.S. and M.S. degrees in applied physics and mathematics from Moscow Institute of Physics and Technology, Dolgoprudny, Russia, in 1989 and 1991, respectively. He joined the Electrical and Computer Engineering Department at the University of California—Riverside in 2011, where he is currently a Research Engineer and an Adjunct Professor. He has coauthored 5 book chapters, more than 70 scientific publications and 7 U.S. patents. He received Inventor Recognition Awards from Microelectronics Advanced Research Corporation in 2006 and 2008.

Guanxiong Liu received the B.S. degree in electronic science and technology from Beijing University of Aeronautics and Astronautics, Beijing, China, in 2007, and the Ph.D. degree in electrical engineering from the University of California—Riverside (UCR), Riverside, CA, USA, in 2012. He spent two years as a Research Scientist in a graphene technology startup company Bluestone Global Tech, working on commercialization of large area graphene. He returned to UCR to continue research of nanodevices implemented with 2-D materials. His research is focused on investigation of charge density wave effects in Van der Waals materials and electronic noise in nanodevices. His expertise includes nanofabrications, device characterization, and electronic applications. He published more than 25 technical papers, including in journals such as *Nature Nanotechnology, Nature Communications*, and *Nano Letters*. Among his honors are the Best Poster Awards at the Materials Research Society Spring Meeting (2016) and SRC-DARPA FAME Review and Workshop (2017).

Alexander A. Balandin (F'13) received the B.S. degree in 1989 and the M.S. degree (*summa cum laude*) in applied physics and mathematics in 1991 from Moscow Institute of Physics and Technology, Dolgoprudny, Russia. He received the second M.S. and Ph.D. degrees in electrical engineering from the University of Notre Dame, Notre Dame, IN, USA, in 1995 and 1997, respectively. From 1997 to 1999, he was a Research Engineer in the Department of Electrical Engineering, University of California—Los Angeles (UCLA). In 1999, he joined the University of California—Riverside (UCR), where he is currently a Distinguished Professor of Electrical and Computer Engineering, the University of California Presidential Chair Professor of Materials Science and Engineering, the Director of the Nano-Device Laboratory (NDL), the Director of the Phonon Optimized Engineered Materials (POEM) Center, an Associate Director of the DOE Energy Frontier Research Center (EFRC) Spins and Heat in Nanoscale Electronic Systems (SHINES) and an Interim Director of UCR.s Nanofabrication Facility. He received The MRS Medal (2013) of the Materials Research Society for his discovery of the unique heat conduction properties of graphene, and the IEEE Pioneer of Nanotechnology Award (2011) for his phonon engineering and nanotechnology research. He is an elected Fellow of the following professional societies: MRS, APS, OSA, SPIE, IOP, IOM3, and AAAS. He is among the Thomson Reuters' Highly Cited Researcher. He serves as the Deputy Editor-in-Chief for *Applied Physics Letters* for nanoscience and nanoengineering fields.